Optimization of GaAs/AlGaAs staircase avalanche photodiodes accounting for both electron and hole impact ionization

A. Pilotto[a,*], C. Nichetti[b,c], P. Palestri[a], L. Selmi[d], M. Antonelli[b], F. Arfelli[c,e], G. Biasiol[f], G. Cautero[b,e], F. Driussi[a], D. Esseni[a], R.H. Menk[b,e,g], T. Steinhartova[c,f]

[a] DPIA, University of Udine, 33100 Udine, Italy
[b] Elettra-Sincrotrone Trieste S.C.p.A, Area Science Park Basovizza, 34149 Trieste, Italy
[c] Department of Physics, University of Trieste, 34128 Trieste, Italy
[d] DIEF, University of Modena and Reggio Emilia, 44100 Modena, Italy
[e] Istituto Nazionale di Fisica Nucleare, INFN Sezione di Trieste, Trieste 34100, Italy
[f] IOM CNR, Laboratorio TASC, Area Science Park Basovizza, 34149 Trieste, Italy
[g] Department of Medical Imaging, University of Saskatchewan, Saskatoon, SK S7N 5A2, Canada

ARTICLE INFO

Keywords:
Staircase avalanche photodiode
Modeling
Nonlocal history-dependent impact ionization model

ABSTRACT

A recently developed nonlocal history dependent model for electron and hole impact ionization is used to compute the gain and the excess noise factor in avalanche photodiodes featuring heterojunctions of III-V compound semiconductors while accounting for both carriers. The model has been calibrated with measurements by our group, as well as on noise versus gain data from the literature. We explore the avalanche photodiode design trade-offs related to the number of GaAs/AlGaAs conduction band steps for X-ray spectroscopy applications.

1. Introduction

Avalanche Photodiodes (APDs) are widely employed as receivers in optical communication systems, X-ray detectors in physics experiments and medical imaging equipments [1–3]. APDs can operate in the linear regime, i.e. with a reverse bias lower than the breakdown voltage, or in Geiger mode, i.e. biased above breakdown. The latter biasing scheme is employed in e.g. Silicon Photo-Multipliers [4], while the linear regime is used e.g. for X-ray detection [5]. We consider in the following APDs working in the linear regime. Their main feature (see Fig. 1) is that the photo-generated current I_{ph} is amplified by an internal gain M provided by impact ionization (II). The stochastic nature of II results in a noise power that deviates by a factor F (denoted as *excess noise factor*) from the intrinsic shot noise due to the Poissonian arrival time of incoming photons.

To optimize the device and predict the optimum bias point, accurate models are needed. Since impact ionization is a markedly nonlocal phenomenon involving high energy carriers, an exact solution of the Boltzmann Transport Equation via, for example, full band Monte Carlo simulations, would be the most appropriate modeling approach [6]. The computational burden can be reduced by using nonlocal numerical models [7–11], where II is described via suitable ionization coefficients α and β (for electrons and holes, respectively) that represent the inverse of the average distance between consecutive II events. These approaches allow users to describe large and complex and devices that would be inefficient to simulate with a full band Monte Carlo simulator.

In this paper, we report APD device optimization based on the newly developed nonlocal history dependent II model of [11]. We analyze APDs featuring a so called *staircase* structure [12], where the multiplication region contains heterojunctions of III-V compound semiconductors and their corresponding ternary alloys. Differently from Multi-Quantum-Well (MQW) APDs that have always abrupt heterojunctions between a low (E_{G1}) and a high (E_{G2}) bandgap material [13,14], in staircase APDs each stage is linearly graded from E_{G1} to E_{G2} and the abrupt discontinuity is only between E_{G2} and E_{G1} [12]. The staircase enhances electron II over hole II, which offers the possibility to achieve a good trade-off between gain and excess noise [7]. The numerical modeling results are compared with simple analytical formulas for the device gain and noise.

This work extends the report in [15] by providing additional results about the relation between the nonlocal model and a compact formula for gain and noise in the presence of hole II. The paper is organized as follows: Section 2 summarizes the nonlocal history dependent II model of [11]. The calibration of the model on GaAs diodes and the

* Corresponding author.
E-mail address: pilotto.alessandro@spes.uniud.it (A. Pilotto).

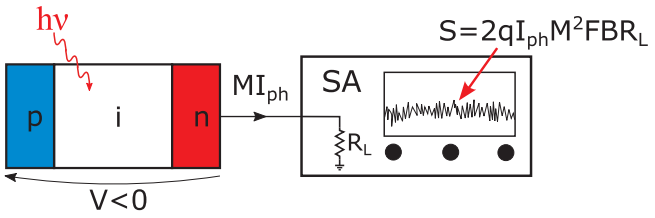

Fig. 1. Sketch of a reverse biased p-i-n APD working in the linear regime connected to a spectrum analyzer. The gain is denoted by M, while F is the excess noise factor. The photo-generated current I_{ph} is amplified by the internal gain M. The noise power spectral density at the output of the analyzer is the current shot noise $2qI_{ph}$ multiplied by the squared gain M^2, the instrument bandwidth B and its input resistance R_L. Moreover the noise is further increased by F that indicates the deviation from pure shot noise.

comparison with experimental data for staircase APDs are reported in Section 3. Simulation results for different number of conduction band steps in staircase APDs based on AlGaAs/GaAs heterojunctions are shown and interpreted in Section 4. Conclusions are drawn in Section 5.

2. Model description

The Energy Balance History Dependent Model (EBHDM) presented in [11] is conceived as a postprocessing of the conduction and valence band profiles ($E_C(x)$ and $E_V(x)$ respectively) firstly obtained using TCAD simulations [16]. The first order energy balance equation in [17] is used to derive a suitable effective field for electrons

$$E_{eff,e}(x|x') = \frac{1}{\lambda_e}\int_x^{x'} \frac{dE_C}{dx}(x'')exp\left(\frac{x''-x'}{\lambda_e}\right)dx'' \quad (1)$$

The II coefficients are expressed as

$$\alpha(E_{eff,e})(x|x') = A_e \cdot exp\left(-\left(\frac{E_{ce}}{E_{eff,e}(x|x')}\right)^{\gamma_e}\right) \quad (2)$$

and similarly for the hole II coefficient. Here the coordinate x is the point where the carrier is gene-rated (optically or by II), while x' is the position where II scattering takes place. The model is history dependent in the sense that at the same position carriers experience a different ionization probability per unit length α and β depending on where they have been generated.

Following [8], probabilistic considerations are then used to derive the average gain M and the excess noise factor F from the α and β profiles: the full expressions can be found in [11].

The model parameters $\lambda_{e,h}$, $A_{e,h}$, $E_{ce,h}$ and $\gamma_{e,h}$ are calibrated on p-i-n APDs, as shown in the next section, and then kept fixed when analyzing more complex staircase structures.

3. Model validation and calibration

As shown in [11], the EBHDM reproduces a variety of experimental data for APDs with different material and architectures. As a relevant example, Fig. 2 reports with filled circles the $F(M)$ curve for a GaAs p-i-n diode [9]: we see that $F \approx 0.75M$, which results in high noise at large M values. This is a consequence of similar electron and hole II coefficients ($\alpha \simeq \beta$) in GaAs (as well as in many other III-V compounds). Note that, although Silicon would be a much better material in this respect ($\alpha \simeq 20\beta$ [12]), III-V semiconductors are still preferable for X-ray detection since they offer a higher detection efficiency (due to the higher atomic number) and APD speed and bandwidth (due to larger carrier velocity) [18]. Fig. 3 reports the calibrated α and β as a function of the field used as input in our model and compares them with data in the literature.

To improve the noise performance of III-V APDs, staircase structures have been proposed, where conduction band discontinuities provide

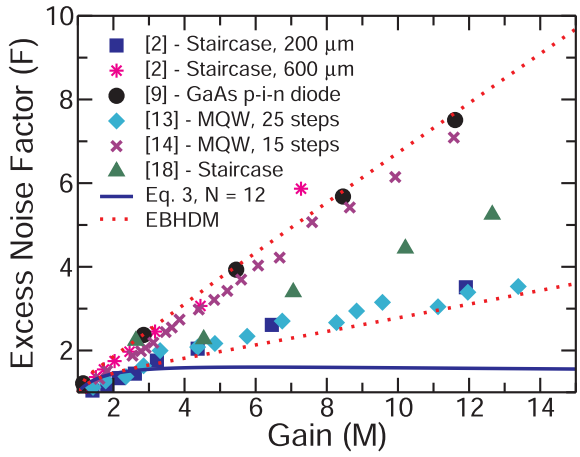

Fig. 2. Excess noise factor as a function of the gain for different GaAs/AlGaAs APDs: experimental data for a thick (W = 1.6 µm) GaAs p-i-n diode from [9] (•), staircase APDs fabricated by our group [2] (■, ✳ for the 200 µm and the 600 µm mesa diameters, respectively), a MQW APD with 25 steps [13] (♦), a MQW APD with 15 steps [14] (x) and for the staircase APD of [18] (▲). The dotted lines represent the results obtained with the EBHDM model (same calibration for both devices), while the solid line is Eq. (3) [12] (for N = 12 steps).

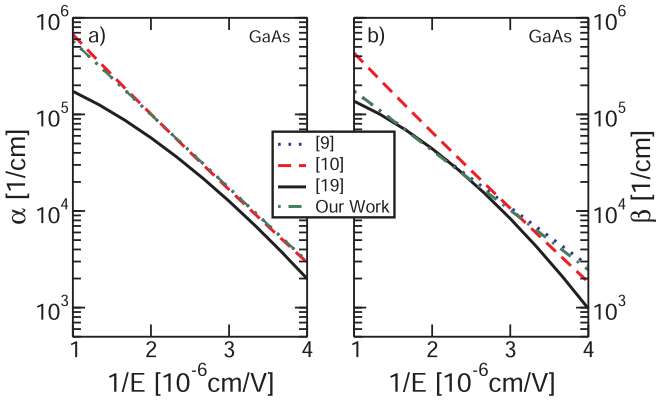

Fig. 3. α (a) and β (b) used to reproduce with the EBHDM the $F(M)$ curves for the GaAs p-i-n diodes reported in [9] (as in Fig. 2) and other sets from the literature [10,19].

extra kinetic energy to electrons crossing them, while valence band discontinuities, opposed to the motion direction, subtract kinetic energy to holes. This increases electron II w.r.t hole II. In the limit case where hole II is negligible, the excess noise factor can be computed as [12]:

$$F(P,N) = 1 + \frac{(1-P)[1-(1+P)^{-N}]}{1+P} \quad (3)$$

where N is the number of multiplication steps (i. e. conduction band discontinuities) and $P = \sqrt[N]{M} - 1$ (that is $M = (P+1)^N$) is the electron's ionization probability per step.

For the staircase APDs in the AlGaAs/GaAs system in [2], the measured $F(M)$ curves for the devices with mesa diameters of 200 µm and 600 µm are reported in Fig. 2. The $F(M)$ curve for the APD with diameter 200 µm is in agreement with the experimental results for the GaAs/AlGaAs MQW APD with 25 steps in [13]: the noise is much lower than for the p-i-n diode and its behavior is predicted also by the EBHDM (that is calibrated on p-i-n diodes without additional model parameter changes when considering staircase structures). The $F(M)$ curve for the device with diameter 600 µm, instead, lies very close to the results reported in [14] for a GaAs/AlGaAs MWQ APD with 15 steps and to the experimental results for the GaAs p-i-n diode [9]. Concerning the difference between the results for the devices in [2], we think that the

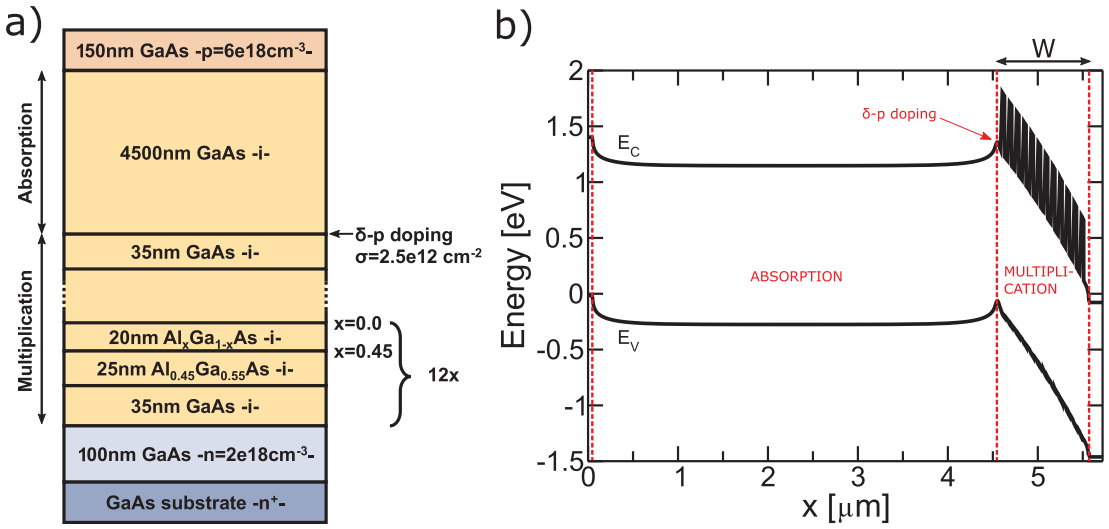

Fig. 4. Structure (a) and band diagram at equilibrium (b) of the staircase APD fabricated in [2]. The main structure consists in an absorption region (on the left) separated from the multiplication region (on the right) by a Dirac's delta p-type doping. The multiplication region is composed by the repetition of 12 heterojunctions between GaAs and AlGaAs layers.

architecture with a bigger mesa area may show additional noise sources other than multiplication noise. However, the experimental $F(M)$ curve for the GaAs/AlGaAs staircase APD of [18], that is similar to the ones of [2], indicates that the use of staircase APDs is beneficial in terms of excess noise factor at a given gain w.r.t. p-i-n diodes. In other words, our nonlocal model (calibrated on GaAs p-i-n diodes) seems to support the experiments in [13] as well as the noise measured in [2] for the device with a smaller diameter.

It is important to note that the use of Eq. (3) (blue line), using $P = \sqrt[N]{M} - 1$, predicts an even lower noise. This can be explained considering that in the GaAs/AlGaAs system the conduction band energy step is small (see the device structure and band diagram in Fig. 4). This requires large applied biases to increase the gain, but, due to the large induced electric field, significant electron and hole multiplication takes place between the steps. We thus believe that hole II between consecutive steps is responsible for the large difference between the experiments (and the EBHDM) and the predictions of Eq. (3) which neglects hole II.

Before continuing, it is worth mentioning that in the EBHDM the sole effect of the heterojunction is to add energy steps equal to the difference in affinity between the materials. Phenomena related to momentum conservation or to disorder at the interface are not included. In practice, in the model the heterojucntion provides energy to the carriers over a short distance, making impact ionization more localized and thus with a reduced associated excess noise.

4. Optimization of GaAs/AlGaAs staircase APDs

Experimental and modeling results in Fig. 2 point out that staircase structures in GaAs/AlGaAs perform much better than GaAs pin diodes in terms of noise at given gain. However the excess noise factor is far from what is expected from Eq. (3), the reason being hole II between the steps due to the large applied electric field, which in turn is necessary to increase the gain because the amplitude of the conduction band discontinuity is relatively small. In this section we analyze whether increasing the number of steps improves the situation.

4.1. EBHDM results for different number of steps

We have considered a device structure in Fig. 4, for different values of the number of steps in the multiplication region. Fig. 5 shows that the excess noise factor for given gain is reduced when the number of steps is

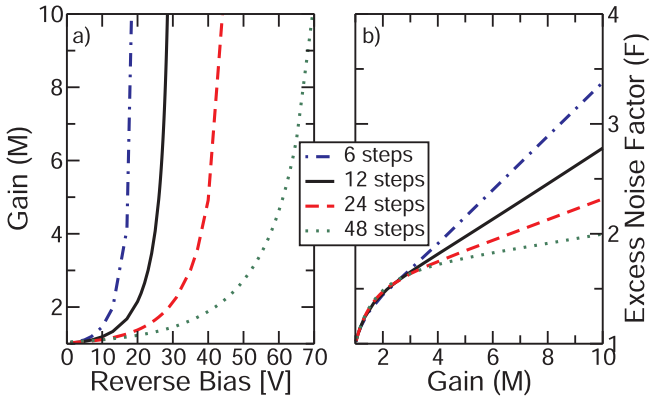

Fig. 5. Simulated (EBHDM) gain as a function of the applied bias (a) and excess noise factor as a function of gain (b) for a staircase APD like the one in Fig. 4 with $N = 6, 12, 24, 48$ multiplication steps.

increased. Furthermore, by increasing the number of steps we achieve high gain over a larger voltage interval, which in turn makes the external biasing of the device much simpler than in the case with few steps, where high gain can be attained only by biasing the device close to breakdown that is, at the edge of the intended linear regime of operation. Of course, with large number of steps high bias voltages are necessary to obtain high gains, but those voltages do not require a very precise setting as with a small number of steps.

The trend in Fig. 5 can be explained by considering that the large number of steps enhances the intrinsic gain that can be achieved without applying an additional electric field. So, for given gain, a structure with more steps entails a lower electric field, as can be seen in Fig. 6.

A quantitative interpretation of the results in Fig. 5, requires models that go beyond Eq. (3) and include hole II, as described in the next subsection.

4.2. Interpretation based on the electron and hole ionization probabilities per step

Analytic expressions to compute the overall gain and excess noise factor in staircase APDs when *both* electrons and holes ionize have been proposed in [20]:

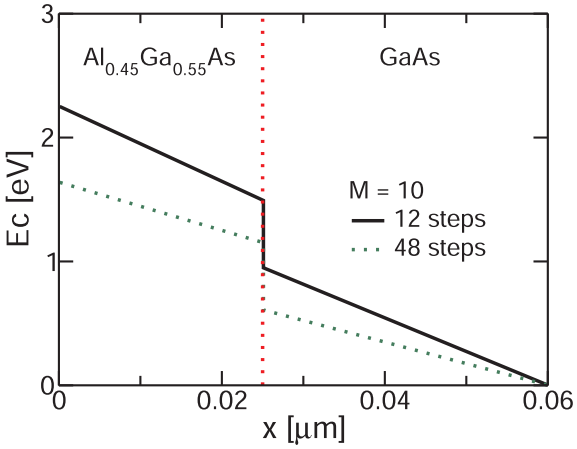

Fig. 6. Conduction band profile of a 0.55 eV single multiplication step (as for the $Al_{0.45}Ga_{0.55}As/GaAs$ [16]) at fixed total gain ($M = 10$) for staircase APDs with 12 (solid line) and 48 steps (dashed line).

$$M(P, Q, N) = \frac{(1+P)^N(1-k)}{(1+kP)^{N+1} - k(1+P)^{N+1}} \tag{4}$$

and

$$F(P, Q, N) = 1 + \frac{(1-1/M)(1-k)}{2+P(1+k)} \times \left\{-P + 2\frac{1-kP^2}{1+kP}\left[Mk\frac{1+P}{1-k} + \frac{1}{1+P}\right]\right\} \tag{5}$$

where P and Q are the electron's and hole's ionization probabilities per step, respectively, and $k = Q/P$. Eqs. (4) and (5) are valid in the low gain limit of the linear regime, when electron and hole impact ionization events at a single step can be treated separately, as if the two mechanisms were independent. Although this may be correct if II is localized at the steps, the accuracy is limited when II events are spread out between the steps.

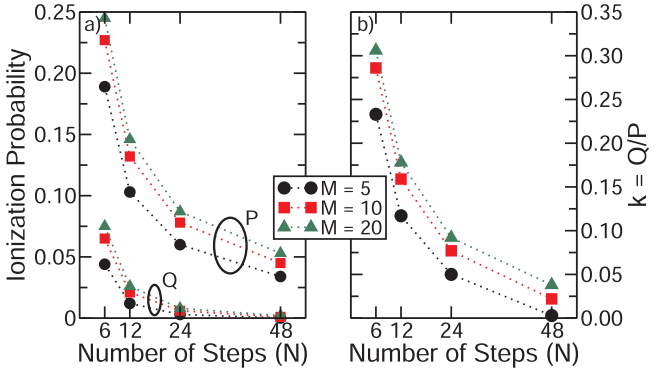

Fig. 8. Simulated (EBHDM) electron's and hole's ionization probabilities (a) and ionization ratio $k = Q/P$ (b) as a function of the number of steps at given gain $M = 5, 10, 20$.

We have extracted P and Q by simulating electron and hole II in single or double step structures that include the region with electric field between the steps. In particular, P is computed from the gain M obtained simulating a single step structure that includes the step and the electric field region just after the step (up to the next step), by activating only electron II and writing $P = M - 1$ (Fig. 7a). To calculate Q two steps (and not only one) should necessarily be included in the simulation domain, because the distance that holes have to travel in order for the II coefficient to be in equilibrium with the electric field is larger than the thickness of a single step (see Fig. 7b). We then compute Q as

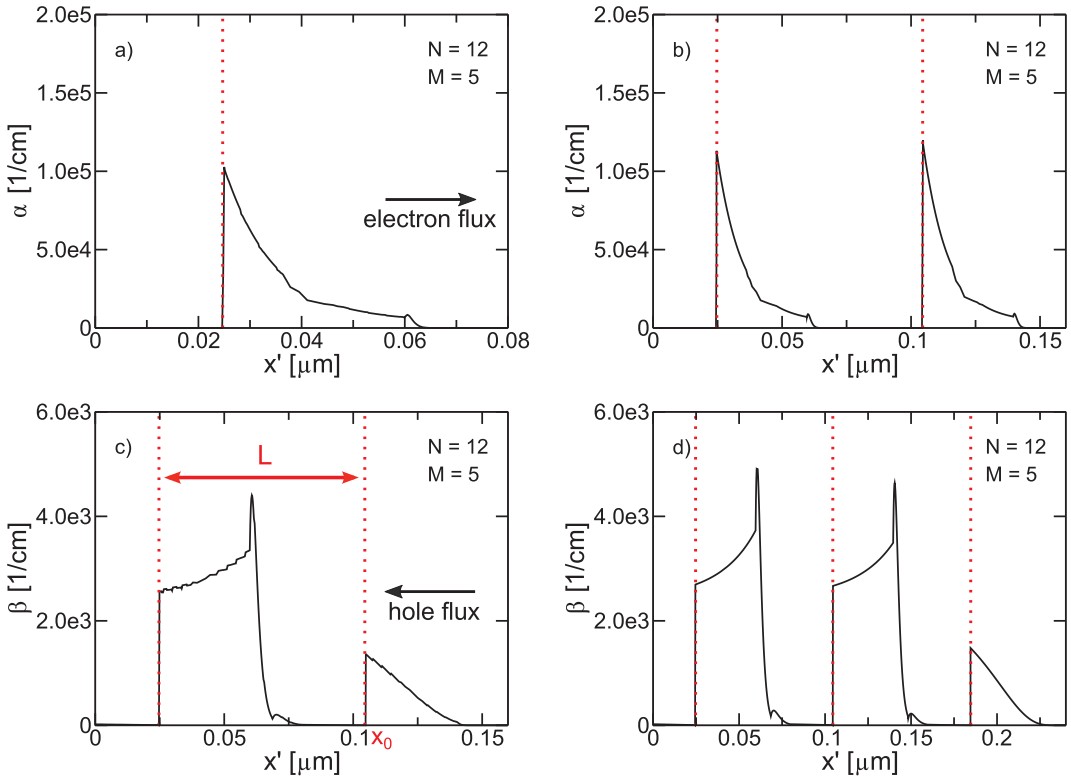

Fig. 7. (a)(b) Electron's impact ionization coefficient $\alpha(0|x')$ and (c)(d) hole's impact ionization coefficient $\beta(W|x')$ as a function of the ionization point x' in one (a), two (b)(c) or three (d) steps of a GaAs/AlGaAs staircase APD ($N = 12$, $M = 5$). $x = W$ is the right-most point of the multiplication region. The location of conduction and valence band discontinuities is highlighted by red dashed lines.

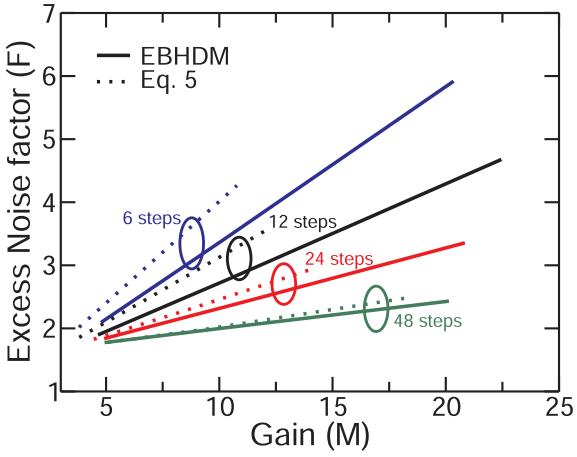

Fig. 9. Comparison of the excess noise factor as a function of the gain computed by using the EBHDM (solid lines) or by using Eqs. (4) and (5) with the P and Q from Fig. 8a (dashed lines) for a staircase APD like the one in Fig. 4 with $N = 6, 12, 24, 48$ multiplication steps.

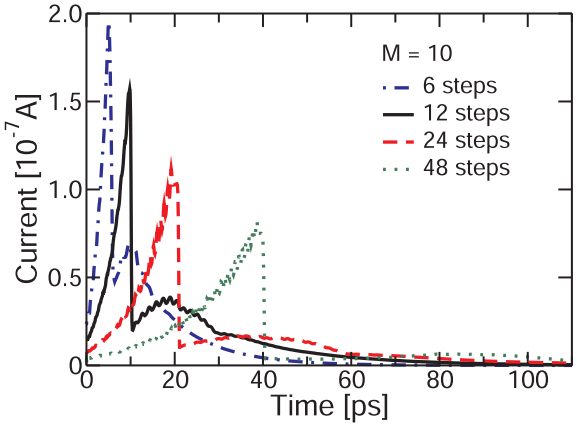

Fig. 10. Simulated current waveforms for a staircase APD like the one in Fig. 4 with $N = 6, 12, 24, 48$ multiplication steps at fixed gain $M = 10$.

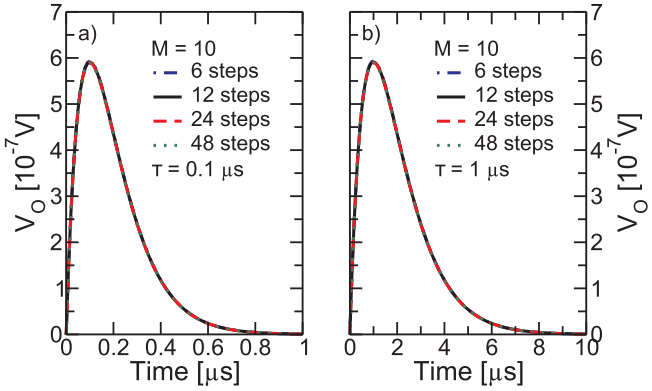

Fig. 11. Simulated current waveforms, after the convolution with the transfer function of a CR-RC shaper with time constant (a) $\tau = 0.1$ μs or (b) $\tau = 1$ μs, for a staircase APD like the one in Fig. 4 with $N = 6, 12, 24, 48$ multiplication steps at fixed gain $M = 10$. Note that the curves in panels (a) and (b) would be essentially the same if plotted as a function of t/τ.

$$Q = exp\left(\int_{x_0-L}^{x_0} \beta(x_0|x')dx'\right) \tag{6}$$

where $L = W/N$ is the length of one multiplication step and only hole II is active in the simulation.

Fig. 8a reports the P and Q obtained with this procedure. P and Q are plotted as a function of N for different gains, which means that for each N the electric field between the steps is set to achieve the desired gain in the complete N-step structure. If we increase the number of steps, the same gain is achieved with a lower electric field between the steps. Thus, both P and Q in Fig. 8a decrease when increasing N. The effect of the reduction of the applied field is much larger on Q than on P (at $M = 10$, from $N = 6$ to $N = 48$, Q is reduced by 98.5%, while P is reduced by 80%), since electrons also feel multiplication by the conduction band steps, whereas valence band discontinuities are negligible. As a result $k = Q/P$ tends to zero for increasing N (Fig. 8b), leading to a structure essentially dominated by electron II.

Fig. 9 compares the EBHDM results of Fig. 5 with the results of Eqs. (4) and (5) using the P and Q values in Fig. 8. The mutual agreement is quite good for $N = 24$ and $N = 48$, while Eq. (5) looses accuracy for a smaller number of steps. In fact, at given gain P and Q are large when N is small; thus the assumption behind Eqs. (4) and (5) that electron and hole ionizations can be treated as independent events becomes less justified. In conclusion, the comparison of the EBHDM and Eqs. (4) and (5) confirms that the main advantage of using a large number of steps is to reduce the electric field necessary to obtain a given gain, thus reducing hole II between the steps.

4.3. Time response

The drawback of an increased number of steps is the longer multiplication region and thus longer time response to single photon absorption. The Random Path Length (RPL) implementation of the EBHDM [21] describes the time evolution of the current pulse and can be used to determine the bandwidth of the APD. The RPL takes as input the impact ionization coefficients, $\alpha(x|x')$ and $\beta(x|x')$ which we take to be exactly the same as used for the computation of the gain and of the excess noise factor with the EBHDM in Sects. 4.1–4.2. Moreover, in all the simulations we assume the same and constant saturated drift velocity for electrons and holes ($v_e = v_h = 10^7$ cm/s [22]), without any dependence on the electric field. Fig. 10 reports current pulses due to single photon absorption for $N = 6$, 12, 24 and 48. They show a retarded peak when increasing N because the carriers must travel over a longer distance. On the other hand, the smaller hole II at large N values reduces the amplitude of the secondary peaks and slows down current tails compared to the amplitude of the main peak. This means that the transient essentially ends when the holes generated by electron II at the last step have traveled back to the first step of the staircase. In the presence of a significant ionization of holes, instead, holes travelling backward generate other electrons that themselves generate additional holes, creating secondary peaks and tails after the main peak.

When considering X-ray spectroscopy as a relevant application, one should remind that the diode current is processed by a leaky integrator followed by an CR-RC shaper. The overall transfer function of the system is approximately $H(\omega) = \frac{Z_0}{(1+j\omega RC)^2}$, where Z_0 is the DC transimpedance of the system. Consequently the output signal is given by the convolution of the current pulses in Fig. 10 with a function $h(t) = A(\frac{t}{RC})exp\left(-\frac{t}{RC}\right)$. Since the time constant $\tau = RC$ is usually in the μs range [23], all the current pulses in Fig. 10 result in essentially the same waveform after the shaper (see Fig. 11).

The above analysis suggests that, for X-ray spectroscopy, increasing the number of steps is beneficial because it reduces the noise at constant gain, hence it improves the energy resolution of the system, which, if the gain is high enough to make negligible the contribution of the readout electronics to the overall noise, is given by $FWHM = 2.35\sqrt{(f+F-1)E\varepsilon}$ [5] (where f is the Fano factor, E is the X-ray photon energy and ε is the electron-hole pair creation energy) and therefore decreases for decreasing F. Moreover, the energy resolution is improved with practically no penalty to the speed of the overall detector.

5. Conclusions

We have investigated the optimization of APDs for X-ray spectroscopy using a nonlocal model for gain, noise and speed in avalanche photodiodes based on III-V compounds and alloys accounting for both electron and hole II. The model points out that increasing the number of conduction band steps in these staircase structures reduces the noise at fixed gain, because a lower electric field between the steps (and thus lower hole II) is required for given gain. The increase in the number of steps does not imply any practical drawback in terms of dynamic response of the system, because the shaper usually has a time constant (set to be as close as possible to the optimum case where the combined noise of the input-referred voltage and current sources of the read-out are minimized [24,25]) much longer than the time delay of the APD.

Acknowledgements

This work was supported by the Italian MIUR through the PRIN 2015 Project under Grant 2015WMZ5C8.

References

[1] Campbell JC, Demiguel S, Ma F, Beck A, Guo X, Wang S, Zheng X, Li X, Beck JD, Kinch MA, Huntington A, Coldren LA, Decobert J, Tscherptner N. Recent advances in avalanche photodiodes. IEEE J Sel Top Quantum Electron 2004;10(4):777–87. https://doi.org/10.1109/JSTQE.2004.833971.

[2] Nichetti C, Steinhartova T, Antonelli M, Cautero G, Menk RH, Pilotto A, Driussi F, Palestri P, Selmi L, Arfelli F, Biasiol G. Gain and noise in GaAs/AlGaAs avalanche photodiodes with thin multiplication regions. J Instrum 2019;14(1). https://doi.org/10.1088/1748-0221/14/01/C01003. pp. C01003–1- C01003–8.

[3] Ren M, Maddox S, Chen Y, Woodson M, Campbell JC, Banks S. AlInAsSb/GaSb staircase avalanche photodiode. Appl Phys Lett 2016;108(8). https://doi.org/10.1063/1.4942370. pp. 081101–1-081101-4.

[4] Renker D. Geiger-mode avalanche photodiodes, history, property and problems. Nucl Instrum Methods Phys Res A 2006;567:48–56. https://doi.org/10.1016/j.nima.2006.05.060.

[5] Tan CH, Gomes RB, David JPR, Barnett AM, Bassford DJ, Lees JE, Ng JS. Avalanche gain and energy resolution of semiconductor X-ray detectors. IEEE Trans Electron Devices 2011;58(6):1696–701. https://doi.org/10.1109/TED.2011.2121915.

[6] Ong DS, Li KF, Plimmer SA, Rees GJ, David JPR, Robson PN. Full band Monte Carlo modeling of impact ionization, avalanche multiplication, and noise in submicron GaAs p+-i-n+ diodes. J Appl Phys 2000;87(11):7885–91. https://doi.org/10.1063/1.373472.

[7] McIntyre RJ. Multiplication noise in uniform avalanche diodes. IEEE Trans Electron Devices 1966;ED-13(1):164–8. https://doi.org/10.1109/T-ED.1966.15651.

[8] McIntyre RJ. A new look at impact ionization – part I: a theory of gain, noise, breakdown, and frequency response. IEEE Trans Electron Devices 1999;46(8):1623–31. https://doi.org/10.1109/16.777150.

[9] Yuan P, Anselm KA, Hu C, Nie H, Lenox C, Holmes AL, Streetman BG, Campbell JC, McIntyre RJ. A new look at impact ionization – part II: gain and noise in short avalanche photodiodes. IEEE Trans Electron Devices 1999;46(8):1632–9. https://doi.org/10.1109/16.777151.

[10] Saleh MA, Hayat MM, Saleh BEA, Teich MC. Dead-Space-based theory correctly predicts excess noise factor for thin GaAs and AlGaAs avalanche photodiodes. IEEE Trans Electron Devices 2000;47(3):625–33. https://doi.org/10.1109/16.

[11] Nichetti C, Pilotto A, Palestri P, Selmi L, Antonelli M, Arfelli F, Biasiol G, Cautero G, Driussi F, Klein NY, Menk RH, Steinhartova T. An improved nonlocal history dependent model for gain and noise in avalanche photodiodes. IEEE Trans Electron Devices 2018;65(5):1823–9. https://doi.org/10.1109/TED.2018.2817509.

[12] Capasso F, Tsang WT, Williams GF. Staircase solid-state photomultipliers and avalanche photodiodes with enhanched ionization rates ratio. IEEE Trans Electron Devices 1983;ED-30(4):381–90. https://doi.org/10.1109/T-ED.1983.21132.

[13] Kagawa T, Iwamura H, Mikami O. Dependence of the GaAs/AlGaAs superlattice ionization rate on Al content. Appl Phys Lett 1989;54(1):33–5. https://doi.org/10.1063/1.100825.

[14] Chia CK, Ng BK, David JPR, Rees GJ, Tozer RC, Hopkinson M, Airey RJ, Robson PN. Multiplication and excess noise in $Al_xGa_{1-x}As$/GaAs multilayer avalanche photodiodes. J Appl Phys 2003;94(4):2631–7. https://doi.org/10.1063/1.1593217.

[15] A. Pilotto, P. Palestri, L. Selmi, M. Antonelli, F. Arfelli, G. Biasiol, G. Cautero, F. Driussi, D. Esseni, R.H. Menk, C. Nichetti, T. Steinhartova, Optimizing the Number of Steps and the Noise in Staircase APDs with Ternary III-V Semiconductor Alloys, Proceedings of EUROSOI-ULIS 2019, pp. to be defined, Apr. 2019.

[16] Sentaurus Device User Guide, Version L-2016.03, Synopsys, Mountain View, CA, USA, 2016.

[17] Goldsman N, Frey J. Efficient and accurate use of the energy transport method in device simulation. IEEE Trans Electron Devices 1988;35(9):1524–9. https://doi.org/10.1109/16.2586.

[18] Lauter J, Forster A, Luth H, Muller KD, Reinartz T. AlGaAs/GaAs avalanche detector array – 1 GBit/s X-ray receiver for timing measurements. IEEE Trans Nucl Sci 1996;43(3):1446–51. https://doi.org/10.1109/23.507080.

[19] Bulman GE, Robbins VM, Brennan KF, Hess K, Stillman GE. Experimental determination of Impact ionization coefficients in (100) GaAs. IEEE Electron Device Lett 1983;EDL-4:181–5. https://doi.org/10.1109/EDL.1983.25697.

[20] Teich MC, Matsuo K, Saleh BEA. Excess noise factors for conventional and superlattice avalanche photodiodes and photomultiplier tubes. IEEE J Quantum Electron 1986;QE-22(8):1184–93. https://doi.org/10.1109/JQE.1986.1073137.

[21] Pilotto A, Palestri P, Selmi L, Antonelli M, Arfelli F, Biasiol G, Cautero G, Driussi F, Menk RH, Nichetti C, Steinhartova T. An improved Random Path Length algorithm for p-i-n and staircase avalanche photodiodes. Proc SISPAD 2018;2018:26–30. https://doi.org/10.1109/SISPAD.2018.8551751.

[22] Ng JS, Tan CH, Ng BK, Hambleton PJ, David JPR, Rees GJ, You AH, Ong DS. Effect of dead space on avalanche speed. IEEE Trans Electron Devices 2002;49(4):544–9. https://doi.org/10.1109/16.992860.

[23] Gomes RB, Tan CH, Meng X, David JPR, Ng JS. GaAs/$Al_{0.8}Ga_{0.2}As$ avalanche photodiodes for soft X-ray spectroscopy. J Instrum 2014;9. https://doi.org/10.1088/1748-0221/9/03/P03014. pp. P03014–1-P03014-10.

[24] Gatti E, Manfredi PF. Processing the signals from solid-state detectors in elementary-particle physics. Rivista del Nuovo Cimento 1986;9(1):1–146. https://doi.org/10.1007/BF02822156.

[25] Fernandes LMP, Amaro FD, Antognini A, Cardoso JMR, Conde CAN, Huot O, Knowles PE, Kottmann F, Lopes JAM, Ludhova L, Monteiro CMB, Mulhauser F, Pohl R, dos Santos JMF, Schaller LA, Taqqu D, Veloso JFCA. Characterization of large area avalanche photodiodes in X-ray and VUV-light detection. J Instrum 2007;2. https://doi.org/10.1088/1748-0221/2/08/p08005. pp. P08005–1-P08005-30.